Spin diffusion in bulk GaN measured with MnAs spin injector

Shafat Jahangir,[1] Fatih Doğan,[2] Hyun Kum,[1] Aurelien Manchon,[2] and Pallab Bhattacharya[1,*]
[1]*Center for Photonics and Multiscale Nanomaterials, Department of Electrical Engineering and Computer Science, University of Michigan, Ann Arbor, Michigan 48109-2122, USA*
[2]*Division of Physical Science and Engineering, King Abdullah University of Science and Technology, Thuwal 23955, Saudi Arabia*
(Received 4 May 2012; revised manuscript received 25 June 2012; published 16 July 2012)

Spin injection and precession in bulk wurtzite *n*-GaN with different doping densities are demonstrated with a ferromagnetic MnAs contact using the three-terminal Hanle measurement technique. Theoretical analysis using minimum fitting parameters indicates that the spin accumulation is primarily in the *n*-GaN channel rather than at the ferromagnet (FM)/semiconductor (SC) interface states. Spin relaxation in GaN is interpreted in terms of the D'yakonov-Perel mechanism, yielding a maximum spin lifetime of 44 ps and a spin diffusion length of 175 nm at room temperature. Our results indicate that epitaxial ferromagnetic MnAs is a suitable high-temperature spin injector for GaN.

DOI: 10.1103/PhysRevB.86.035315 PACS number(s): 85.75.−d, 75.76.+j

I. INTRODUCTION

Semiconductor spintronics has been the focus of attention for its applicability in high-performance logic, memory, and optoelectronic devices. The wide-band-gap III-V semiconductor GaN, which generally crystallizes in the hexagonal wurtzite (w) structure, has gathered much interest as a promising material for spintronics due to its room temperature ferromagnetism when doped with rare-earth metals (e.g., manganese),[1] and also its weak spin-orbit coupling (SOC) which results in long spin-relaxation times. GaN also shows attractive optoelectronic properties in the visible spectrum range, making it suitable for spin-light emitting diodes (spin-LEDs) and lasers. Therefore, it is important to study and develop efficient spin injectors and spin dynamics in GaN materials. Much of the spin dynamics in a given semiconductor is governed by several spin-dependent relaxation mechanisms, which is a direct consequence of spin-orbit interactions of the spin-polarized electrons with its surrounding environment.

Spin-orbit coupling is the most fundamental spin-dependent interaction present in nonmagnetic semiconductor materials, which determines the coherence time of spin-polarized carriers. The three possible spin-relaxation mechanisms present in w-GaN structures have been identified as (1) D'yakonov-Perel' (DP), (2) Elliot-Yafet (EY), and (3) electron-electron (-hole) scattering. The DP mechanism is present in materials without structural inversion symmetry, such as zincblende structures, but is also present in bulk wurtzite materials due to the hexagonal *c* axis which results in a spontaneous piezoelectric polarization. The spin splitting of the conduction band due to this inversion asymmetry of the crystal lattice manifests as an effective momentum-dependent magnetic field, producing an effect similar to the Rashba-type SOC that is linear in **k** (electron momentum). The EY relaxation mechanism causes spin flip through scattering events with impurities or phonons, but have been largely neglected as a possible source of spin relaxation in w-GaN as discussed later. Finally, the electron-electron (-hole) scattering may become dominant in highly doped materials at low temperatures and potentially enhance the spin relaxation time.[2] The design of efficient spin-based semiconductor devices requires clear identification of relevant spin-relaxation mechanisms involved as well as the demonstration of spin injection in the bulk of the semiconductor channel.[3] In particular, strong spin relaxation at the interface between the injector and the semiconductor channel dramatically affects the performance of spin devices.[4]

Previous studies on spin-relaxation mechanisms in GaN by optical measurements, such as time-resolved Faraday rotation and time-resolved Kerr rotation, have shown that the DP mechanism is the dominant spin-relaxation mechanism.[5,6] In this study we report electrical spin injection and detection in bulk w-GaN using an epitaxially grown MnAs/AlAs ferromagnetic tunnel contact in the three-terminal Hanle geometry. The measurements were carried out in a broad temperature range of 10–300 K and across several samples with different doping densities. Rigorous theoretical analysis using minimum fitting parameters show good agreement with experimentally derived spin lifetimes, indicating that the majority of spin accumulation is occurring in the channel rather than at the interface states. Doping dependent spin lifetime measurements point toward the same conclusion.

II. EXPERIMENT

The heterostructure and dimensions of the grown sample are shown in Fig. 1(a). The heterostructure consists of a 500 nm thick Si doped *n*-GaN bulk channel grown on a semi-insulating *c*-axis sapphire substrate with a 5 μm GaN template on top, a 1 nm thick AlAs tunnel barrier (TB) grown by molecular beam epitaxy (MBE) at a substrate temperature of 700 °C, and a 35 nm thick ferromagnetic MnAs spin injector/detector grown at a low-substrate temperature of 250 °C. Three samples were grown, each with a different doping density (sample A: 4.2×10^{17} cm^{-3}, sample B: 1×10^{18} cm^{-3}, sample C: 7.8×10^{18} cm^{-3}). Before growth, the native oxides were removed from the GaN template by dipping the substrate into aqueous HCl (1:1) for 15 min. The substrate was baked at 900 °C prior to growth to remove impurities. The sample was fabricated into multiple three-terminal devices using standard optical lithography with each of the three contacts having a dimension of 200×150 μm^2. With reference to Fig. 1(a), contacts 1 and 3 are remote ohmic (Ti/Au) reference contacts and contact 2 is the ferromagnetic MnAs spin injector/detector. The distance between contacts 1 and 2 (and 2 and 3) is approximately

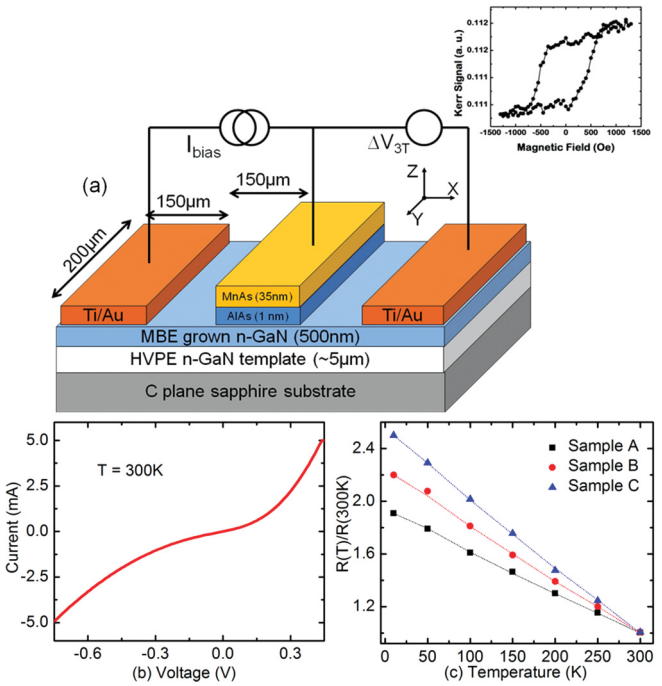

FIG. 1. (Color online) (a) Schematic illustration of the device heterostructure and three-terminal Hanle measurement scheme. Inset shows the in-plane hysteresis characteristics of MnAs grown on GaN. (b) Typical I-V characteristics of the tunneling FM/SC contact. (c) Zero-bias resistance as a function of temperature for samples A, B, and C, indicating tunneling nature of the FM contact.

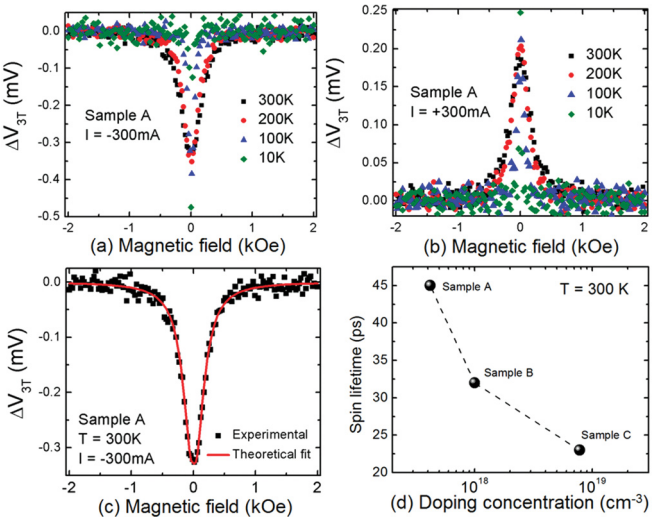

FIG. 2. (Color online) Hanle precession characteristics for spin (a) injection and (b) extraction as a function of temperature. (b) Lorentzian fit to experimental data of sample A at 300K. (c) Spin lifetimes at $T = 300$ K for samples A, B, and C, derived from analysis of measured data.

150 μm, which is much greater than the expected spin diffusion length in our GaN channel. The devices were wirebonded on a chip carrier and loaded into a cryostat between the poles of an electromagnet. The inset to Fig. 1(a) shows the measured magnetic hysteresis characteristics of a 35 nm MnAs film grown on GaN using the magneto-optic Kerr effect (MOKE) technique. The measurement indicates an in-plane easy axis of magnetization for the MnAs contact.

To ensure that the MnAs/AlAs heterojunction provides a tunneling contact, the zero-bias resistance (ZBR) was measured as a function of temperature. A typical I-V characteristic of the fabricated devices is shown in Fig. 1(b). The weak temperature dependence of the ZBR is regarded as a proof of single-step tunneling transport. The $R_0(10\text{ K})/R_0(300\text{ K})$ ratios did not exceed an order of magnitude for all three samples, verifying the tunneling nature of the MnAs/AlAs contact [Fig. 1(c)].

III. RESULTS, ANALYSIS, AND DISCUSSION

Three-terminal Hanle measurements were performed with the bias configuration shown in Fig. 1(a) across a temperature range of 10–300 K. This technique measures the spin accumulation and precession directly beneath the magnetic tunnel barrier contact interface.[3,4,7] A constant dc current is passed through contacts 1 and 2, while the voltage is measured across contacts 2 and 3 as a magnetic field perpendicular to the sample plane (B_z) is swept across the device. The MnAs contact is magnetized parallel to the plane of growth prior to sweeping B_z. The spin accumulation due to injection causes a splitting of the spin-dependent electrochemical potential ($\Delta\mu = \mu_{\text{up}} - \mu_{\text{down}}$), which is detected as a voltage (ΔV_{3T}) across terminals 2 and 3. A perpendicular magnetic field (B_z) across the device precesses the accumulated spin at the Larmor frequency $\omega_L = g\mu_B B_z/\hbar$, resulting in precessional dephasing of the net spin accumulation in the channel, where g is the Lande g factor ($g = 1.94$ for GaN),[5] μ_B is the Bohr magneton, and $\hbar$ is the reduced Planck's constant. However, since the three-terminal measurement technique primarily detects spin accumulation directly beneath the FM contact, localized interface states may cause spin to accumulate at the ferromagnet (FM)/semiconductor (SC) interface rather than the semiconducting channel, leading to erroneous overestimation on the spin lifetime and diffusion length (as pointed out by Tran *et al.*[4]). Therefore, it is necessary to provide evidence that the measured spin accumulation is in the channel rather than at the interface states. As shown later, the doping dependent spin lifetimes indicate that the spin accumulation is predominantly in the channel.

The three-terminal Hanle voltage ΔV_{3T} as a function of B_z for sample A is shown in Figs. 2(a) and 2(b) for the same current bias across contacts 1 and 2, measured at various temperatures. These data are used to calculate the spin lifetime at each temperature. Figure 2(a) corresponds to the case of spin injection, whereas Fig. 2(b) corresponds to spin extraction. The Lorentzian Hanle curves can be analyzed with the equation $V_{3T}(B_z) = \Delta V_{3T}(0)/[1 + (\omega_L \tau_s)^2]$, where the spin relaxation time τ_s is used as a fitting parameter. $\Delta V_{3T}(0)$ is the voltage across contacts 2 and 3 at zero B_z. The fit is shown for sample A in Fig. 2(c) for 300 μA current bias. Similar analysis yields spin lifetimes of ~44, 31, and 22 ps at 300 K for samples A, B, and C, respectively [Fig. 2(d)]. The distinct change in spin lifetime with channel doping is in reasonable agreement with trends of lifetimes measured by optical techniques[5,6] and electron spin resonance measurements.[8]

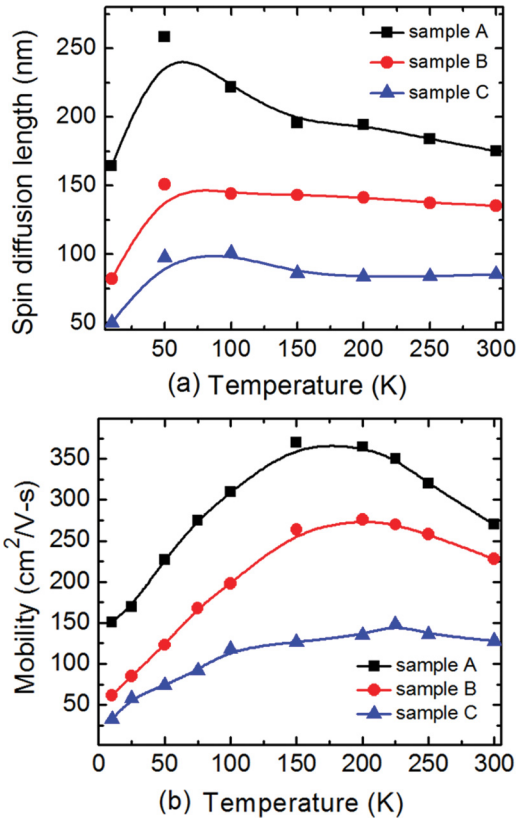

FIG. 3. (Color online) Spin diffusion length as a function of temperature for samples A, B, and C. Solid lines are guides to the eye.

Figure 3(a) shows the spin diffusion length $L_{\rm sd} = (\mu_e k_B T \tau_s/q)^{1/2}$ as a function of temperature calculated with the measured values of τ_s and μ_e. It is observed that the diffusion length increases as the temperature increases from 10 to 50 K, then decreases toward 300 K. This trend can be explained by considering the variation of mobility (μ_e) and spin-relaxation time (τ_s) as a function of temperature for our samples, which are shown in Figs. 3(b) and 5 (dots), respectively. We derive a spin-diffusion length of approximately 180, 140, and 80 nm at room temperature for samples A, B and C, respectively, demonstrating that practical devices with MnAs as spin injectors into GaN may be realized with conventional lithography and fabrication techniques.

Several spin-relaxation mechanisms which determine the spin lifetime in bulk wurtzite structures have been investigated.[2] As mentioned previously, EY and DP mechanisms are dominant in semiconductors with inversion asymmetry. The EY mechanism describes randomization of spin direction by scattering with impurities or phonons, which is given by

$$\frac{1}{\tau_\varepsilon^{\rm EY}} \cong \left(\frac{\Delta_{\rm SO}}{\Delta_{\rm SO}+E_g}\right)^2 \left(1-\frac{m^*}{m}\right)^2 \left(\frac{\varepsilon}{E_g}\right)^2 \frac{1}{\tau_P}, \qquad (1)$$

where $\Delta_{\rm SO}$ is the spin-orbit coupling, E_g is the semiconductor energy band gap, m^*/m is the ratio of the effective/free electron mass, ε is the energy of the electron, and τ_p is the momentum scattering time. The DP mechanism describes spin randomization due to both precession (as result of Rashba and Dresselhaus spin-orbit coupling) and scattering, where the direction of spin precession changes via momentum scattering. The two spin-orbit coupling effects are the consequence of an intrinsic inversion asymmetry present in wurtzite structures. The spin-scattering time of the DP mechanism is given by

$$\frac{1}{\tau_\varepsilon^{\rm DP}} = \frac{4\tau_P}{3\hbar^2}\left[\alpha^2\left(\frac{2m^*\varepsilon}{\hbar^2}\right) + \frac{2}{5}\alpha\beta_3(b-4)\left(\frac{2m^*\varepsilon}{\hbar^2}\right)^2 + \frac{7(4-b)^2+8(1+b)^2}{175}\gamma_3\beta_3^2\left(\frac{2m^*\varepsilon}{\hbar^2}\right)^3\right], \qquad (2)$$

where α is the Rashba coupling parameter including the linear Dresselhaus component, β_3 is the cubic Dresselhaus coefficient, and b is the interference factor between Rashba and Dresselhaus components. For GaN, the interference is negligibly small for the purposes of this analysis and the expected value of $b = 3.959$ (Ref. 9) is approximated as $b = 4$.

Equations (1) and (2) can be expanded to analyze the experimentally derived spin lifetime values as a function of doping and temperature, expressed as[11]

$$\frac{1}{\tau_s^{\rm EY}} \cong \left(\frac{\Delta_{\rm SO}}{\Delta_{\rm SO}+E_g}\right)^2 \left(1-\frac{m^*}{m}\right)^2 \left(\frac{k_B T}{E_g}\right)^2 \times \frac{1}{\tau_P}\frac{I_{\upsilon+2.5}(\beta\mu)I_{1.5}(\beta\mu)}{I_{\upsilon+1.5}(\beta\mu)I_{0.5}(\beta\mu)} \qquad (3)$$

and

$$\frac{1}{\tau_s^{\rm DP}} = \frac{4\tau_P}{3\hbar^2}\left[\alpha^2\left(\frac{2m^*k_BT}{\hbar^2}\right)\frac{I_{1.5}(\beta\mu)}{I_{0.5}(\beta\mu)} + \gamma_3\beta_3^2\left(\frac{2m^*k_BT}{\hbar^2}\right)^3\frac{8I_{\upsilon+3.5}(\beta\mu)I_{1.5}(\beta\mu)}{7I_{\upsilon+1.5}(\beta\mu)I_{0.5}(\beta\mu)}\right], \qquad (4)$$

where $I_d(\beta\mu)$ is the energy convolution of the scattering mechanism, with respect to the Fermi energy μ,

$$I_d(\beta\mu) = \beta^{d+1}\int_0^\infty x^d \frac{e^{-\beta x+\beta\mu}}{(1+e^{-\beta x+\beta\mu})^2}dx \qquad (5)$$

and υ depends on the type of source causing the scattering. The temperature dependence reduces to a well-known quadratic dependence for EY and linear/cubic for DP mechanism above the Fermi temperature (T_F) while saturating to a constant value below T_F for both mechanisms. The temperature range of our experiment covers both sides of the Fermi temperature for samples A and B, but below T_F for sample C. To our knowledge, this is the first theoretical description of spin-relaxation mechanisms in wurtzite GaN over such a wide range of temperature with experimental verification. An earlier work[12] considered only the high- or low-temperature extremes of Eq. (4).

Analysis of the experimental results for all three samples is discussed next. Both EY and DP relaxation mechanisms are caused by temperature-dependent scattering mechanisms, which can be identified by calculating the momentum scattering time from temperature-dependent mobility measurements [Fig. 3(b)]. In most studies, the momentum scattering time (τ_p) is assumed to be constant, which is a valid assumption if the temperature range of the analysis is small and near room temperature. However, for the larger temperature range considered in this study, the temperature dependence of τ_p cannot

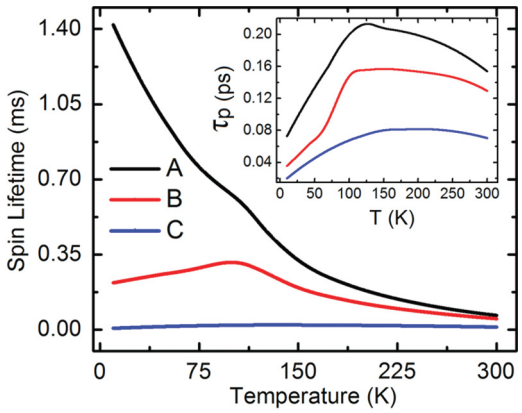

FIG. 4. (Color online) Expected spin lifetime values within the EY spin-relaxation framework. Inset shows the momentum scattering time (τ_p) as a function of temperature for samples A, B, and C.

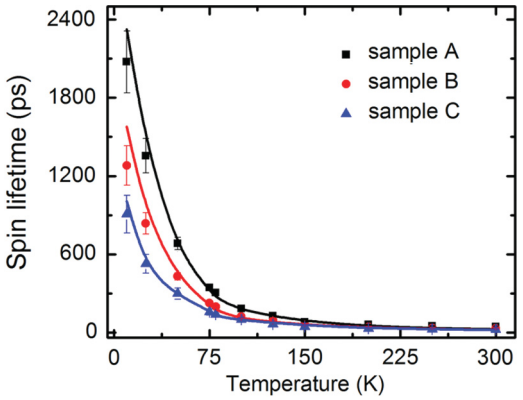

FIG. 5. (Color online) Estimated value of relaxation time within the DP framework for each sample with free-fitting parameters. Experimental values are also plotted along with their error ranges.

be neglected. In the low temperature regime (below 100 K), the momentum scattering time is proportional to temperature; at higher temperatures, it is almost independent of temperature followed by a slightly decreasing trend (inset of Fig. 4). From this we deduce that the relevant scattering mechanisms are ionized impurity scattering in the low-temperature regime and acoustic phonon scattering at higher temperatures.[13] The values of γ_3 and ν used for spin-relaxation calculations in the high- and low-temperature regimes are 6 and 1 (Ref. 2) for γ_3, and 3/2 and 1/2 (Ref. 14) for ν, respectively. The separate contributions from each scattering mechanism are combined as

$$\frac{1}{\tau} = \frac{1}{\tau_{\nu=3/2}} + \frac{1}{\tau_{\nu=1/2}}. \tag{6}$$

The calculated EY spin relaxation times using standard parameters for w-GaN given in Table I and Eq. (3) are shown in Fig. 4. The relaxation times are of the order of milliseconds, which is unreasonable. Therefore, we conclude that the DP relaxation mechanism is dominant in this system and the EY mechanism does not play any significant role.

Calculated spin lifetimes in accordance with the DP mechanism for each sample are shown in Fig. 5 alongside the measured data. The fitting parameters (T_F, α, and β_3) used for each sample are listed in Table II. Both Rashba and Dresselhaus parameters are of the order of their expected values for GaN, and increase with increasing density of carriers. This analysis, however, does not accurately describe the true physical effects, as the values of the Rashba and Dresselhaus parameters should remain constant regardless of the doping concentration. Furthermore, we find that the values of T_F used in the analysis are an order of magnitude lower than theoretically predicted values of this parameter. The latter can be calculated assuming a free-electron model, which is valid for systems at or near the metallic regime, using the equation

$$T_F = \frac{1}{k_B}\frac{\hbar^2}{2m^*}(3\mu n_D)^{2/3}. \tag{7}$$

The calculated values of T_F are listed in Table III. Both uniform distribution of states in momentum space and parabolic bands are assumed in this calculation. We note that the doping concentration in samples B and C is near the metallic regime, while sample A is in the insulating regime. An "effective" Fermi temperature ($T_{F,\mathrm{eff}}$) is estimated for each sample by analyzing the measured spin lifetimes, keeping both the Rashba and Dresselhaus parameters constant at $\alpha = 0.25$ meV nm and $\beta_3 = 0.25$ meV nm^3, obtained from analysis of the measured spin lifetime data. $T_{F,\mathrm{eff}}$ values of 24, 160, and 600 K are obtained for samples A, B, and C, respectively. It is evident that the value of $T_{F,\mathrm{eff}}$ gets closer to the calculated T_F with increasing doping concentration as the system moves closer towards the metallic regime. However, as mentioned previously, the samples analyzed here are all below the metallic regime; hence, the effective T_F values are lower than the calculated T_F values, especially for sample A.

The calculated values of the spin lifetimes using the values of $T_{F,\mathrm{eff}}$ mentioned above are shown alongside the measured data in Fig. 6. While there is reasonable agreement in general, there is an obvious discrepancy in the case of sample C in the temperature regime below 100 K. In this range, the temperature

TABLE I. General GaN parameters used for theoretical calculations.

Parameter	GaN
Band gap (E_g) (eV)	3.4 (Ref. 15)
Spin-orbit coupling (Δ_{SO}) (meV)	20 (Ref. 16)
Effective mass (m^*)	0.2 (Ref. 16)
Rashba coefficient (α) (meV nm)	0.9 (Ref. 9)
Cubic Dresselhaus (β_3) (meV nm^3)	0.32 (Ref. 9)

TABLE II. Parameters used for analyzing data shown in Fig. 5.

Parameter	Sample A	Sample B	Sample C
T_F (K)[a]	45.5	65.2	90.5
α (meV nm)	0.19	0.31	0.46
β_3 (meV nm^3)	0.32	0.32	0.4

[a]Fermi temperature values obtained as a free fitting parameter.

TABLE III. Calculated expected and effective Fermi temperatures for each sample as a function of doping density.

Sample	Density (10^{17}cm^{-3})	$T_{F,\mathrm{exp}}$ (K)[a]	$T_{F,\mathrm{eff}}$ (K)[b]
A	4.2	118.9	24
B	10	212	160
C	78	834	600

[a]Calculated Fermi temperature using Eq. (7).
[b]Effective Fermi temperature estimated from analysis shown in Fig. 6.

is (with respect to the effective Fermi temperature) low enough to freeze most of the carriers, leaving only the temperature dependence of τ_p in the model used here. In this temperature range, localized scattering with impurities[10] and carrier-carrier scattering[2] become dominant.

IV. CONCLUSION

From the dependence of spin lifetime on the doping, as well as the good agreement between experimental results and theory with minimum fitting parameters, we conclude that spin accumulation and precession is occurring primarily in the GaN channel. Our observed values of spin lifetime, as well as its variation with doping and temperature, are consistent with previously reported values obtained from optical measurements.[5,6] We have shown that the DP mechanism explains spin relaxation in w-GaN bulk systems over a wide range of temperatures. The free-electron model is not valid at low-carrier densities but becomes applicable as the system approaches the metallic regime. The doping dependent spin lifetime and the agreement between measured and calculated values of the spin lifetime with very few fitting parameters in the analysis provide strong evidence that the observed spin accumulation is in the GaN channel rather than at localized states.

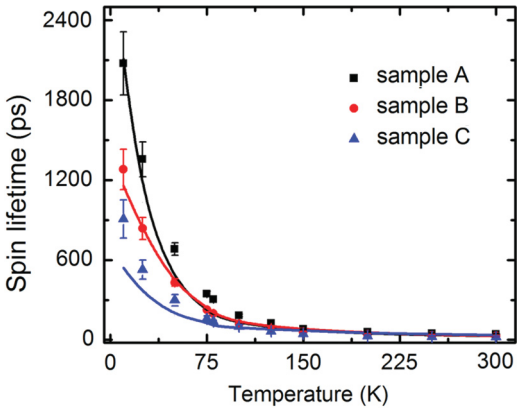

FIG. 6. (Color online) Estimated value of relaxation time within the DP framework. The Rashba and cubic Dresselhaus parameter values used are $\alpha = 0.25$ meV nm and $\beta_3 = 0.25$ meV nm^3, respectively. Resulting effective Fermi temperatures are 24, 160, and 600 K for samples A, B and C, respectively. Experimental values are also plotted along with their error ranges.

ACKNOWLEDGMENTS

This work is supported by the National Science Foundation, MRSEC Program, under Grant 0968346 and KAUST under Grant N012509-00.

*pkb@eecs.umich.edu

[1]G. Bouzerar, T. Ziman, and J. Kudrnovsky, Euro Phys. Lett. **69**, 812 (2005).
[2]M. W. Wu, J. H. Jiang, and M. Q. Weng, Phys. Rep. **493**, 61 (2010).
[3]C. H. Li, O. M. J. Van't Erve, and B. T. Jonker, Nat. Commun. **2**, 245 (2011).
[4]M. Tran, H. Jaffres, C. Deranlot, J. M. George, A. Fert, A. Miard, and A. Lemaıtre, Phys. Rev. Lett. **102**, 036601 (2009).
[5]B. Beschoten, E. Johnston-Halperin, D. K. Young, M. Poggio, J. E. Grimaldi, S. Keller, S. P. DenBaars, U. K. Mishra, E. L. Hu, and D. D. Awschalom, Phys. Rev. B **63**, 121202 (2001).
[6]J. H. Buß, J. Rudolph, F. Natali, F. Semond, and D. Hägele, Phys. Rev. B **81**, 155216 (2010).
[7]S. P. Dash, S. Sharma, R. S. Patel, M. P. de Jong, and R. Jansen, Nat. Lett. **462**, 491 (2009).
[8]W. E. Carlos, J. A. Freitas Jr., M. A. Khan, D. T. Olson, and J. N. Kuznia, Phys. Rev. B **48**, 17878 (1993).
[9]J. Y. Fu and M. W. Wu, J. Appl. Phys. **104**, 93712 (2008).
[10]N. J. Harmon, W. O. Putikka, and R. Joynt, Phys. Rev. B **81** 085320 (2010).
[11]N. J. Harmon, W. O. Putikka, and R. Joynt, Appl. Phys. Lett. **98**, 073108 (2011).
[12]J. H. Buß, J. Rudolph, S. Starosielec, A. Schaefer, F. Semond, Y. Cordier, A. D. Wieck, and D. Hägele, Phys. Rev. B **84**, 153202 (2011).
[13]P. Y. Yu and M. Cardona, *Fundamentals of Semiconductors Physics and Materials Properties* (Springer, Berlin, 2010).
[14]J. Kainz, U. Rossler, and R. Winkler, Phys. Rev. B **70**, 195322 (2004).
[15]O. Mayrock, H.-J. Wunsche, and F. Henneberger, Phys. Rev. B **62**, 16870 (2000).
[16]http://www.ioffe.rssi.ru/SVA/NSM/Semicond/GaN/.